Axisymmetric convective states of pure and binary liquids enclosed in a vertical cylinder and boundary conditions' influence thereupon

Accepted for publication in *Physics of Fluids*

E. Millour[a], G. Labrosse[a] and E. Tric[b]

[a] Université Paris-Sud,
Laboratoire d'Informatique pour la Mécanique
et les Sciences de l'Ingénieur LIMSI-CNRS,
BP 133, 91403 ORSAY CEDEX, FRANCE

[b] Université Nice Sophia Antipolis,
Laboratoire Géosciences AZUR,
250 rue Albert Einstein, 06560 VALBONNE, FRANCE

Abstract

The high Rayleigh number (Ra) axisymmetric convection regimes of $Pr = 1$ pure and ($Le = 0.1$, $\Psi = -0.2$) binary liquids are numerically investigated and compared. The fluids are enclosed in a vertical cylinder, of aspect ratio $\frac{\text{height}}{\text{radius}} = 2$ and heated from below, with either no-slip or free-slip kinematic lateral boundary conditions. Branches of solutions and transitions between states that occur as Ra is varied up to $\mathcal{O}(10^5)$ are given, along with a description of the encountered bifurcations. When a free-slip condition is imposed along the circumference of the cell, pure fluid and binary liquid stationary flows are found to become identical at high Ra, an often reported feature. When the lateral boundary condition is set to no-slip, the high Ra steady flows of pure and binary liquid, although very similar, undergo different bifurcations. This is related with a locally quasi-quiescent region present in both cases, the stability of which controls the flow regime in the whole fluid layer. A branch of resulting oscillatory states thus does not appear in the bifurcation diagram of the binary liquid.

1 Introduction

Fluid motion driven by thermal gradients is a common feature of many natural and industrial systems. The traditional problem of a mono-component fluid layer heated from below is a paradigm of the rich spatiotemporal behaviors that can arise in non-linear systems driven away from equilibrium. Since the governing equations are well known and the experimental setup is sufficiently simple to allow controlled experiments, it has become the context of many studies (see for instance [2] for a review of recent developments) on pattern formation and related topics. The 'simplicity' of this system comes from the fact that only two parameters are needed to describe it, the Prandtl Pr and Rayleigh Ra numbers. The first solely depends on the characteristics of the fluid whereas the second is the control parameter, proportional to the temperature difference applied to the layer. The typical evolution of the system with increasing Ra is well known. The layer first remains motionless for too small an applied temperature difference. As the latter is increased, it eventually exceeds a critical value (Ra_c) where steady convection sets in. More complicated dynamics, such as time-dependent convection, arises as the system is taken further away from onset.

In two-component miscible liquid mixtures, mass fraction and temperature gradients are coupled by the Soret effect [3]. According to the sign thereof (or equivalently of the non-dimensional parameter it enters in, the separation ratio Ψ), the solute (which we take to be the heaviest of the two components) migrates towards either the warmer ($\Psi < 0$) or colder ($\Psi > 0$) part of the container. The resulting Soret-driven mass fraction gradient thus induces a solutal buoyancy that strengthens (when $\Psi > 0$) or opposes ($\Psi < 0$) the thermal one, consequently rushing or delaying the onset of convection, comparatively to the pure fluid problem. When thermal and solutal buoyancies compete, the interplay between the two moreover typically [3, 4, 5] leads to the following dynamical behavior:

1. As in the pure fluid problem, the quiescent state is stable for Ra smaller than a threshold value Ra_H.

2. At Ra_H, a subcritical Hopf bifurcation of the quiescent state occurs and finite amplitude oscillatory convection sets in.

3. Once reached, the branch of oscillatory solutions can be followed towards higher or lower values of Ra. Most studies on binary liquid convection focus on these states and their spatiotemporal properties (see, among the multitude of published theoretical, experimental and numerical works, [4, 6], as well as [5] for a recent review).

4. For a high enough Ra value (typically less than twice Ra_H) the oscillations cease as a transition to steady overturning convection (SOC) occurs.

Investigations of the stationary solutions of the system generally do not extend to Ra values much greater than those at which the transition to SOC occurs. It is indeed often noticed (e.g. [5, 7, 8]) that for increasing thermal stress (i.e. increasing Ra), the steady convective flows of binary mixtures become similar to those of 'equivalent' $\Psi = 0$ pure fluids. This behavior reflects the fact that strong convective motion efficiently mixes the mass fraction of solute in the bulk of the system, thus weakening any compositional effect on its solutions. This feature has been used to develop a model, based on the assumption that a binary mixture problem can be seen as a perturbation of a pure fluid one, to predict the transition to SOC [8]. Experimental results [9] however, do not support these theoretical predictions.

There is also an experimental study [10] which unambiguously shows that the stationary convective patterns that develop in a binary liquid are unlike those obtained in a pure fluid subjected to identical constraints. The aim of this paper is to tackle a similar topic, as to whether pure liquid and binary fluid convection are indeed alike at high Ra.

The present work only deals with axisymmetric solutions of the problem for reasons exposed in [11] where it is shown that, in small aspect ratio cylinders, lateral kinematic boundaries conditions exert a significant influence on binary liquid flow dynamics. Only a pure fluid and a particular binary liquid are considered, both such that $Pr = 1$. It will be seen that their convection at high Ra display similarities as well as discrepancies and that the occurrence of either, once again, depends on the lateral kinetic boundary condition (no-slip or free-slip) along the cylinder's circumference.

This paper is organized as follows. The main features of the mathematical model, along with numerical accuracy assessments, are stated in Section 2. Results obtained for both types of fluids, and both sets of boundary conditions, are given and analyzed in Section 3. Our conclusions are then summarized in Section 4.

2 Mathematical model

2.1 Parameters and boundary conditions

The set of reference scales and corresponding dimensionless equations ruling incompressible binary liquid convection are given in [11]. The physical fields are the velocity $\mathbf{v} = u\mathbf{e_r} + w\mathbf{e_z}$, $\mathbf{e_r}$ and $\mathbf{e_z}$ being the radial and upward unit vectors, θ and γ, the departures from the static dimensionless temperature ($\Theta_S(z)$) and reduced mass fraction ($\Gamma_S(z)$) profiles.

The parameters of the problem are the thermal Rayleigh number, Ra, the Prandtl Pr and Lewis Le numbers and the separation ratio Ψ. In this study we consider $Pr = 1$ fluids, the binary mixture being such that $Le = 0.1$ and $\Psi = -0.2$.

We consider an axisymmetric cylindrical enclosure of aspect ratio $\frac{\text{radius}}{\text{height}} \equiv \frac{R}{H} = \frac{1}{2}$ with the same boundary conditions as in [11]. We just recall that, along the adiabatic cylinder's circumference, we shall investigate both cases of either no-slip or free-slip constraints:

$$\text{(NS)} \quad u = w = 0 \text{ for } \; r = \frac{1}{2}\,,$$

or

$$\text{(FS)} \quad u = \frac{\partial w}{\partial r} = 0 \text{ for } \; r = \frac{1}{2}\,.$$

The first (NS) refers to a liquid enclosed in a cylindrical box whereas the last (FS) is a crude approximation (capillary effects being here discarded) of a straight liquid bridge [12].

2.2 Numerical method

A description of the pseudo-spectral numerical code used in this study is given in [11]. It is thus merely recalled here that a Chebyshev pseudo-spectral method and a second order finite difference schemes are used to solve the spatial and temporal evolutions of the fields.

All forthcoming results were obtained using grids of 51×101 collocation nodes in $r \times z$. This spatial resolution, shown to be sufficient for low Ra computations [11], is likewise sufficient over the range of Ra investigated in this paper. This spatial accuracy was assessed by re-computations of a few solutions (which include steady and unsteady flows, as well as at the highest values of Ra) using refined 81×161 grids.

For the four investigated systems (pure fluid or binary liquid, in the NS or FS configurations), the time step δt required to accurately compute the various solutions needed to be decreased with increasing Ra. For instance, computations of binary liquid flows began at low Ra with $\delta t = 3 \times 10^{-4}$ but the $Ra = 2 \times 10^5$ oscillatory state was obtained with $\delta t = 10^{-5}$. Again, occasional test re-computations of solutions (at a given Ra, using smaller values of δt) were performed in order to assess the good temporal resolution of the obtained flows.

To conclude the accuracy assessment of our computations, note that for the pure fluid (in the NS configuration), the threshold for the onset of convection is found to occur at $Ra = 10871$, in good accordance with the linear stability results ($Ra = 10887.15$) of [13].

2.3 Symmetry properties of the solutions

Because of the up-down symmetry of the system, if a state $X_1 = (u_1,\, w_1,\, \theta_1,\, \gamma_1)$ satisfies the balance equations, then so will its 'mirror-image' $X_2 = (u_2,\, w_2,\, \theta_2,\, \gamma_2)$, given by

$$\begin{aligned} u_2(r,z,t) &= u_1(r,-z,t), \\ w_2(r,z,t) &= -w_1(r,-z,t), \\ \theta_2(r,z,t) &= -\theta_1(r,-z,t), \\ \gamma_2(r,z,t) &= -\gamma_1(r,-z,t). \end{aligned}$$

The corresponding transformation is denoted $\mathcal{M}$. Unless invariant under $\mathcal{M}$, solutions therefore come in pairs.

Periodic solutions (of period τ) may possess a temporal symmetry $\mathcal{T}$ relating solutions separated by half a period in the following way:

$$\begin{aligned} u(r,z,t+\tau/2) &= u(r,-z,t), \\ w(r,z,t+\tau/2) &= -w(r,-z,t), \\ \theta(r,z,t+\tau/2) &= -\theta(r,-z,t), \\ \gamma(r,z,t+\tau/2) &= -\gamma(r,-z,t). \end{aligned}$$

3 High Ra dynamics

3.1 FS configuration

Computations were run for both pure fluid and binary mixture for Ra values up to 3×10^5 (over thirty times the threshold values of the corresponding quiescent states).

The evolution with Ra of the pure fluid case is straightforward: once the supercritical pitchfork bifurcation of the quiescent state is reached ($Ra = 6.271 \times 10^3$), steady convection sets in and holds for all Ra (at least up to $Ra = 3 \times 10^5$). Moreover, the convective pattern is found to barely evolve over the investigated Ra interval: flows always consist of a single roll that fills the whole of the enclosure.

The binary liquid sequence of transitions, from the Hopf bifurcation of the rest state to oscillatory convection (along with the complex sequence of bifurcation these solutions undergo) and to steady convection are detailed in [11]. The branch of stationary states, born at a saddle-node bifurcation (at $Ra = 8.117 \times 10^3$) extends up to at least $Ra = 3 \times 10^5$. These flows, as their pure fluid analogues, moreover also consist of a single roll that fills the whole of the enclosure.

At high Ra, binary liquid stream function and temperature fields are strikingly similar to those obtained for the pure fluid (at the same value of Ra). A measure that illustrates the similarity between the pure fluid and binary liquid solutions is the global kinetic energy of the corresponding flows, $E_k(Ra) = \int\limits_{(\Omega)} \frac{\mathbf{v}^2}{2} d\Omega$, plotted in Fig. 1.

As expected, with increasing Ra the strong convective motion in the whole of the enclosure efficiently evens the mass fraction of solute in the bulk of the enclosure, and thus damps any Soret-induced gradient. Consequently, the binary liquid then behaves as a pure fluid in the same conditions.

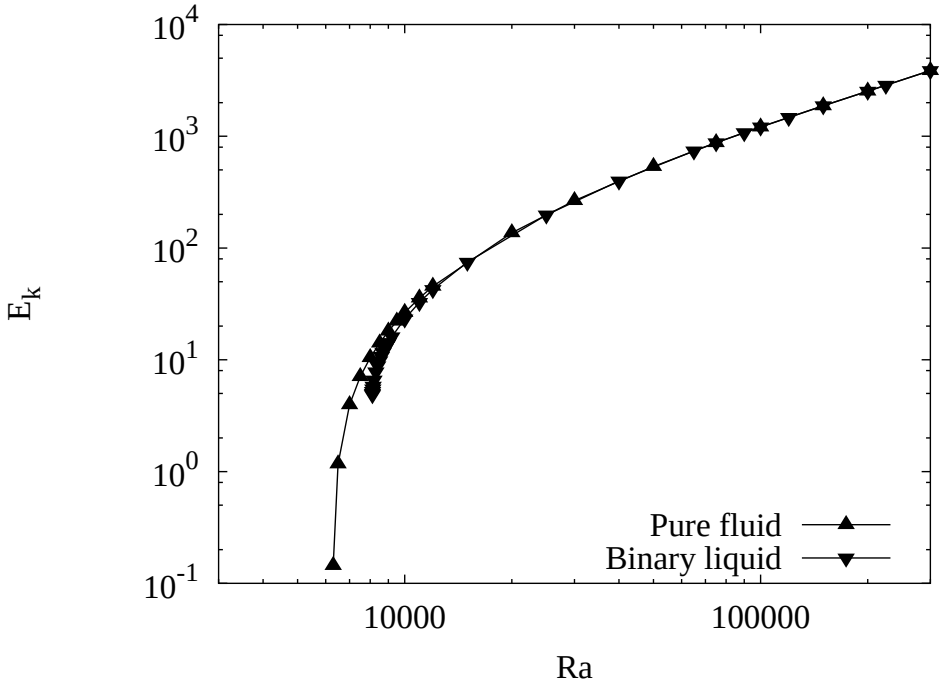

Figure 1: Global kinetic energy E_k of pure fluid and binary liquid steady convective states in the FS configuration.

3.2 NS configuration

When the cylinder's circumference is taken to be a rigid wall, the system displays, for both pure and binary liquids, a wider range of dynamical behavior than in the FS configuration. The pure fluid and binary liquid convective states that occur in the NS configuration are sketched in Fig. 2, along with the ranges in Ra over which they are stable. A complementary $E_k(Ra)$ plot, where all solutions are gathered, is given in Fig. 3

As shown by Figs. 2 and 3, multiple branches of solutions coexist, as not only do both steady and periodic motion occur, but also because two distinct flow patterns arise: either one roll or an $\mathcal{M}$-invariant pair of stacked rolls. The branches of solutions are hence labelled by a subscript referring to the pattern type (one roll or two) it belongs to.

Before giving a detailed description of all the transitions between the various convective regimes, we first comment the main similarities and differences between the pure fluid and binary liquid solutions.

- Each branch of the binary liquid convective states has its analogue in pure fluid, except for the osc_1 flows. This major discrepancy is thoroughly analyzed and discussed in forthcoming Sections.
- For all analogous branches of solutions, bifurcations occur at higher values of Ra in the binary liquid system. This feature reflects the stabilizing effect that one would intuitively expect in a $\Psi < 0$ mixture.
- Transitions in pure fluid from one state (of a given pattern) to its oscillatory counterpart are forward, whereas there is hysteresis in all the transitions in the binary liquid system.

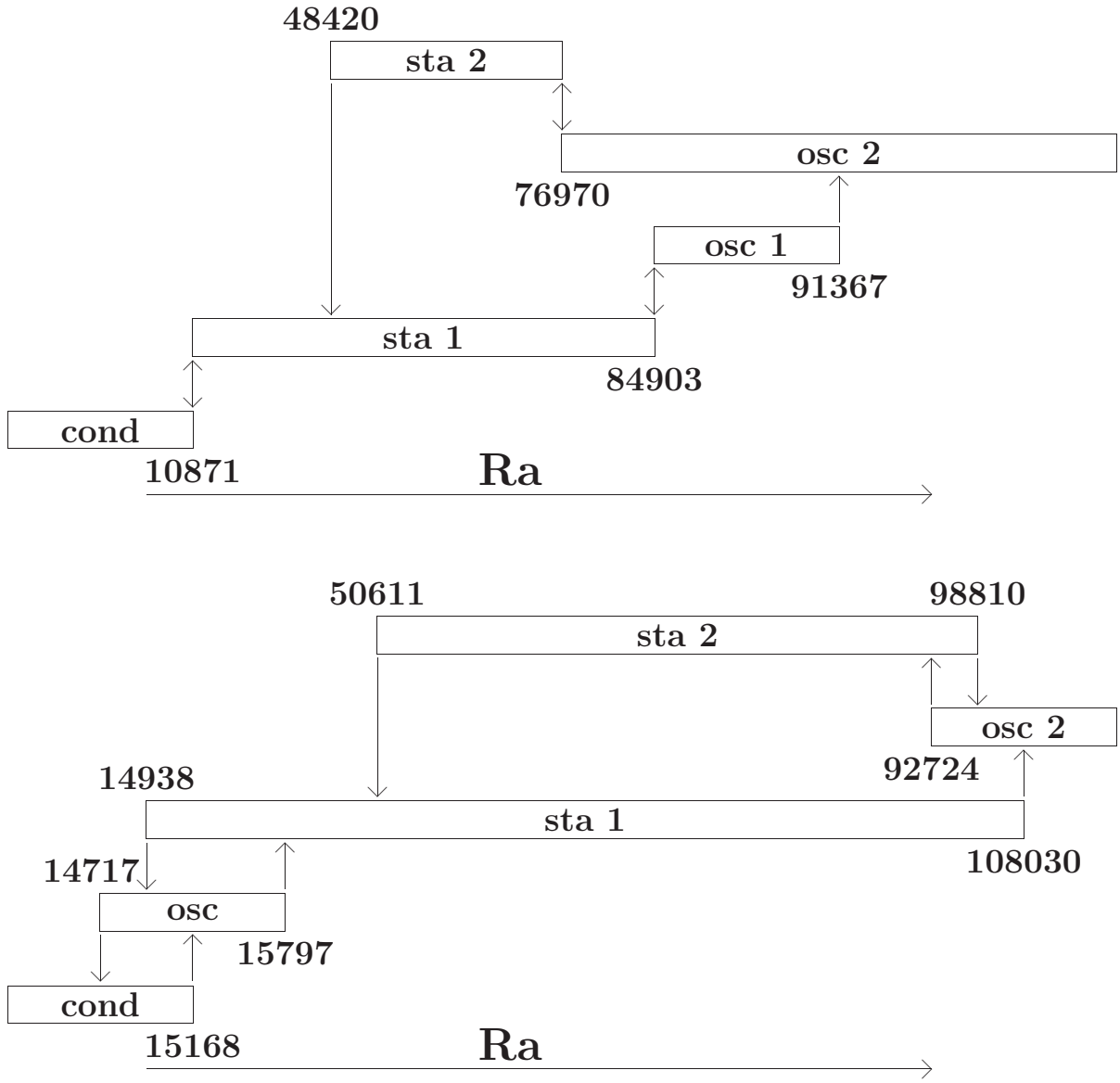

Figure 2: Sketch of the branches of solutions for the pure fluid (top half of the diagram) and binary liquid (lower half of the diagram) in the NS configuration. The arrows indicate the transitions between branches as Ra is increased or decreased beyond or below the given threshold values.

3.2.1 Pure fluid states and transitions

As depicted in Fig. 2, the sta_1 branch that stems from the supercritical pitchfork bifurcation of the quiescent state (at $Ra = 1.0871 \times 10^4$) extends up to $Ra_h = 8.4903 \times 10^4$ where it gives way (via a global bifurcation detailed in Section 3.2.2) to oscillatory convection. The angular frequencies ω of the resulting osc_1 solutions are plotted in Fig. 4. The osc_1 branch extends up to $Ra = 9.1367 \times 10^4$ where it ends in a saddle-node bifurcation. Increasing Ra beyond this threshold leads the system to settle on the osc_2 branch. These states basically consist of oscillations about sta_2-like solutions : during the first half of the period, one of the rolls expands until it fills a large part of the enclosure and then shrinks back to its original position; opposite motion occurs over the second half of the period (osc_2 solutions possess the $\mathcal{T}$ symmetry property). The evolution of the angular frequency of these flows with Ra is given in Fig. 5. These oscillations are of much higher frequency than those of

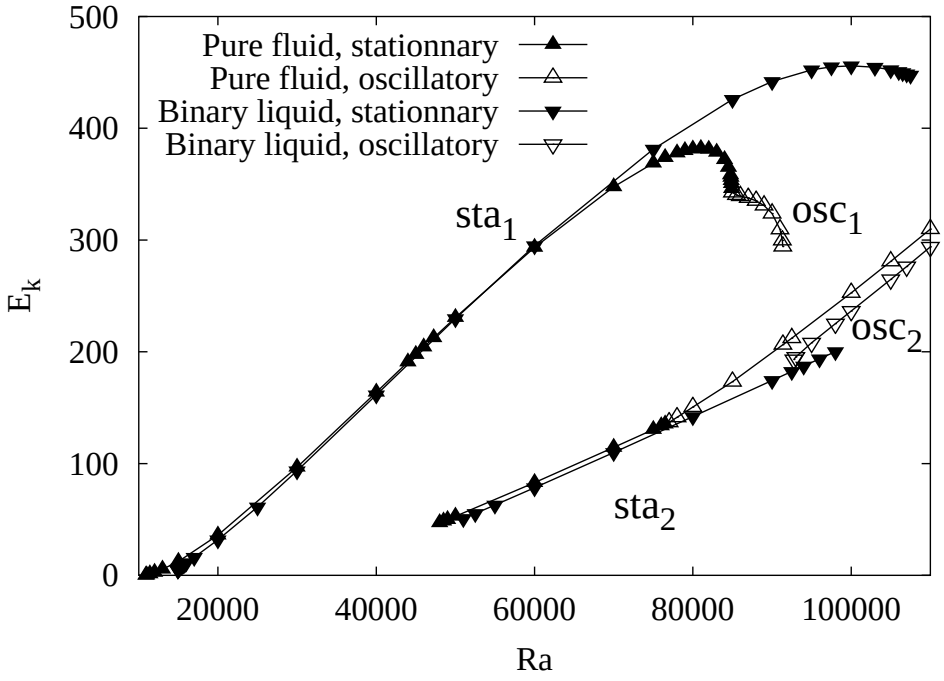

Figure 3: Global kinetic energy E_k of the pure fluid and binary liquid convective states in the NS configuration. The upper curves (sta_1 and osc_1) correspond to single roll flows and the lower ones (sta_2 and osc_2) to stacked rolls states. For oscillatory solutions, the mean value $\frac{1}{\tau}\int_0^\tau E_k(t)dt$ is plotted. Transitions from and to the various branches of solutions are given in Fig. 2.

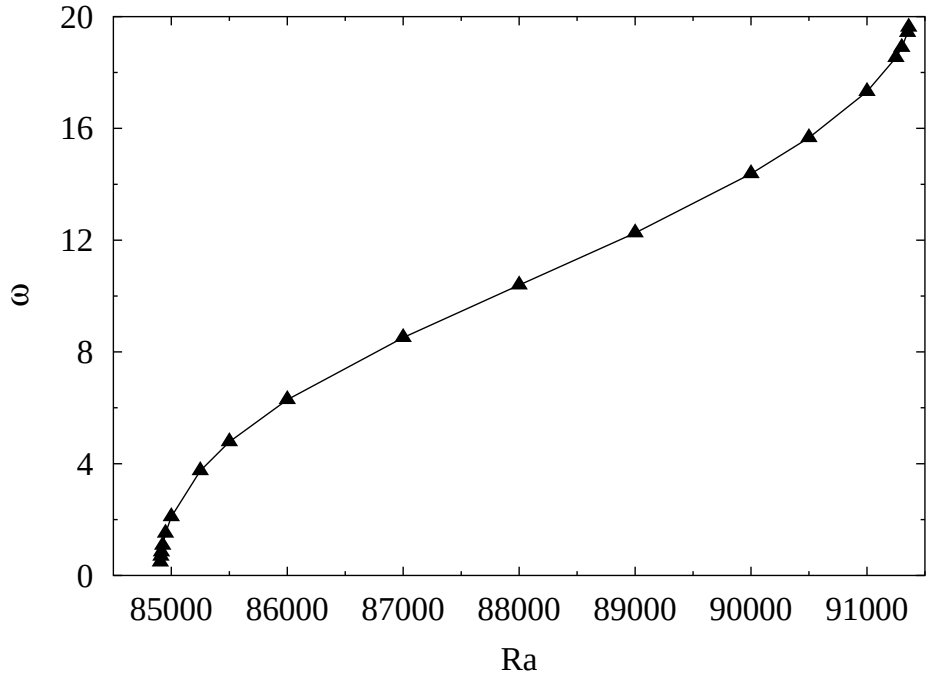

Figure 4: Angular frequency ω of the pure fluid flows along the osc_1 branch of solutions (NS configuration).

the osc_1 solutions and likewise increase with increasing Ra. The osc_2 branch of solutions extends at least up to $Ra = 2 \times 10^5$ and down to $Ra = 7.697 \times 10^4$ as the transition (a

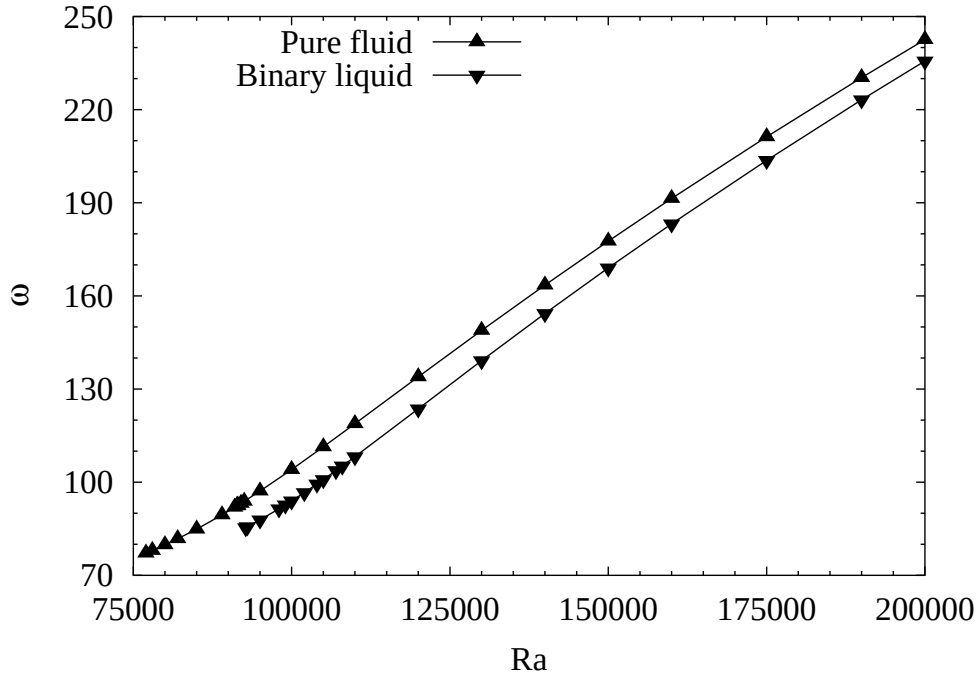

Figure 5: Angular frequencies ω of pure fluid and binary liquid flows along the osc_2 branches of solutions (NS configuration).

supercritical Hopf bifurcation, with $\omega = 77.13$ Hopf frequency) to the sta_2 branch of solutions is reached. The latter can be followed down to $Ra = 4.842 \times 10^4$ where it ends in a subcritical Hopf bifurcation. The destabilizing Hopf mode consists of an alternating circulation (which possesses the $\mathcal{T}$ symmetry property) of fluid that spans the whole enclosure. Due to the subcritical nature of the bifurcation, these low frequency ($\omega = 21.23$ at the bifurcation) oscillations grow exponentially in intensity and eventually cast the system to the sta_1 branch of solutions (Fig. 2).

3.2.2 End of the pure fluid sta_1 branch

Flows of the sta_1 branch of solutions consist of a single roll pattern. Note that such flows are not $\mathcal{M}$-invariant and thus come in $\mathcal{M}$-related pairs. Apart from the main roll, a small roll, located in the 'corner' of the enclosure (where horizontal and side walls meet) is also present for all Ra. At low Ra, these rolls (which will from now on be referred to as corner rolls) are extremely small. The corner rolls however grow in size with increasing Ra, which will be further commented in Section 3.2.5. An example of such flows, the most extreme (at $Ra = 8.49 \times 10^4$, very slightly before the termination of the sta_1 branch), is given in Fig. 6.

As the critical value $Ra_h = 8.4903 \times 10^4$ is reached, the sta_1 state gives way to the oscillatory osc_1 one. The typical evolution of the periodic osc_1 flows above this threshold is illustrated in Fig. 7. The oscillations mainly consist of alternate sequences of slow and rapid evolutions, the former occurring when the system is in the vicinity of 'ghosts' of the pair of sta_1 states and the latter as it is cast from one to the other. The evolution of the system during such switches is given in Fig. 8. The osc_1 oscillations possess the $\mathcal{T}$ symmetry property.

The scenario that leads to the birth of the osc_1 state from the sta_1 ones via a global

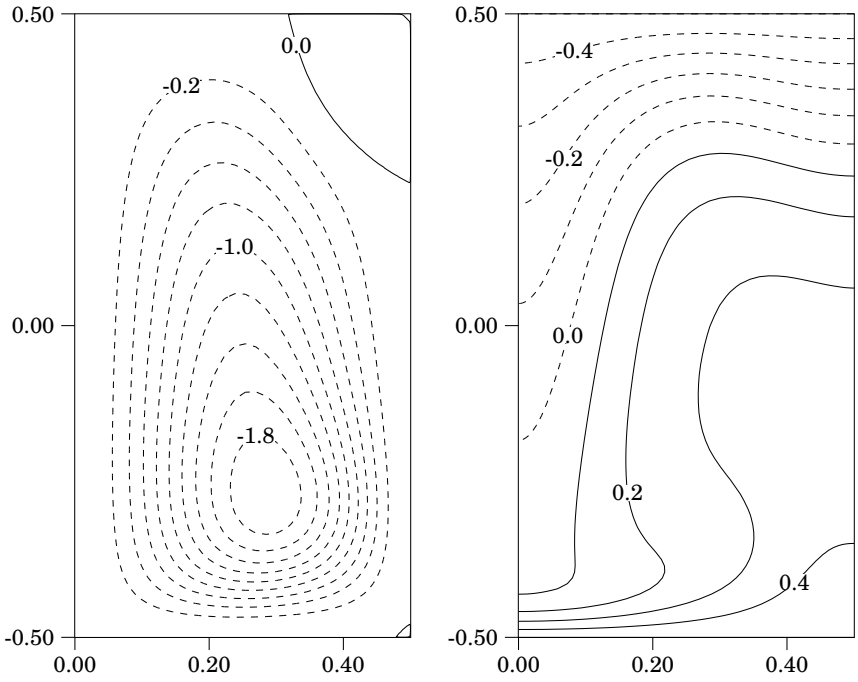

Figure 6: Stream function and temperature $T = \Theta_S(z) + \theta(r,z)$ contours of the $Ra = 8.49 \times 10^4$ pure fluid sta_1 steady state (NS configuration).

bifurcation is sketched in Fig. 9. For values of Ra lower than Ra_h, two pairs of stable (solid dots) and unstable (hollow dots) steady states coexist in phase space, all connected in a heteroclinic orbit. As Ra increases towards Ra_h, stable and unstable states approach one another (pairwise) and merge in a saddle-node bifurcation at $Ra = Ra_h$. The heteroclinic connection between the steady states becomes the osc_1 limit cycle when $Ra > Ra_h$. Although unstable states are unreachable (by our time-marching numerical tool), their presence and the scenario mentioned above are supported by the following observations:

- There is no hysteresis in this transition.
- The (asymptotic) transient behavior of any monitored variable of the sta_1 flows, as they settle towards their final values, clearly display a non-oscillatory exponential relaxation $e^{\lambda t}$. Evaluating the decay rates λ as Ra_h is approached yields the $\lambda(Ra) \propto (Ra_h - Ra)^{1/2}$ scaling expected in the vicinity of saddle-node bifurcations.
- As shown by the $\omega(Ra)$ plot of Fig. 4, the period τ of the oscillations diverges as Ra is decreased towards Ra_h. Slightly above Ra_h (although only over a rather narrow range, $Ra - Ra_h \sim 100$), the evolution of the frequency of the flows follows a $\omega(Ra) \propto (Ra - Ra_h)^{1/2}$ trend.

This global bifurcation has been reported before [14, 15], in the context of axisymmetric thermal convection in a cylinder of larger ($\Gamma = 5$) aspect ratio. These studies moreover include an investigation of the consequences of the sidewall's thermal conductivity on the states and transitions of the system. They show that this bifurcation to oscillatory convection requires a lateral wall that must be a good thermal conductor, which does not correspond to our lateral thermal conditions.

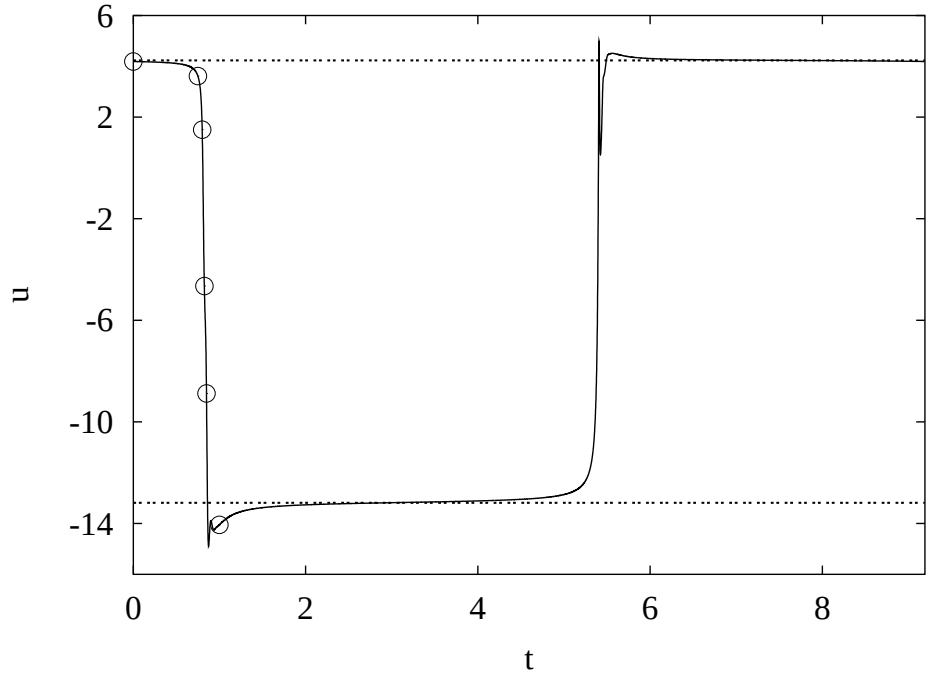

Figure 7: Pure fluid, NS configuration. Temporal evolution of the horizontal velocity u at $r = 0.121$, $z = -0.268$. Dashed lines: $Ra = 8.490 \times 10^4$ sta_1 steady states values. Solid line: time series over a period ($\tau = 9.1910392$) of the $Ra = 8.491 \times 10^4$ osc_1 flow. The hollow dots indicate the instants corresponding to the snapshots displayed in Fig. 8.

3.2.3 Binary liquid states and transitions

The steady sta_1 binary liquid convective states are similar to those of the pure fluid case as they also consist of a single roll. There even is a common range ($Ra \in [3 \times 10^4, 7 \times 10^4]$, as shown by the collapse of the curves in Fig. 3) where both pure fluid and binary liquid systems display very similar velocity and temperature distributions. Beyond this range, a discrepancy (discussed in the next section) between the two arises. The sta_1 branch extends up to $Ra_c = 1.0803 \times 10^5$.

Beyond that last critical value, the flow is cast to the osc_2 branch. Again, these flows are analogues of those encountered in the pure fluid case and are likewise found to be stable at least up to $Ra = 2 \times 10^5$. The osc_2 branch can be followed down to $Ra = 9.2724 \times 10^4$ where it ends in a saddle-node bifurcation which leads the system to settle on the sta_2 branch. If Ra is then increased, the flow remains steady up to $Ra = 9.881 \times 10^4$ where a subcritical Hopf bifurcation (of $\omega = 89.67$ Hopf frequency) leads the system back to the osc_2 branch. There is thus hysteresis in transitions between sta_2 and osc_2 solutions for the binary liquid. The sta_2 branch can be followed down to $Ra = 5.0611 \times 10^4$, where it ends in a subcritical Hopf bifurcation. The destabilizing Hopf mode (of $\omega = 17.49$ Hopf frequency) is strikingly similar to the one that arises in pure fluid (described in Section 3.2.1).

3.2.4 End of the binary liquid sta_1 branch

As mentioned in Section 3.2.3, pure and binary liquid sta_1 convective regimes are similar over $Ra \in [3 \times 10^4, 7 \times 10^4]$ and then differ. The similarity is illustrated by Figs. 6 and 10 which respectively depict pure fluid and binary liquid sta_1 flows slightly before the termination of these branches of solutions. Despite their similarity with pure fluid sta_1 solutions, the

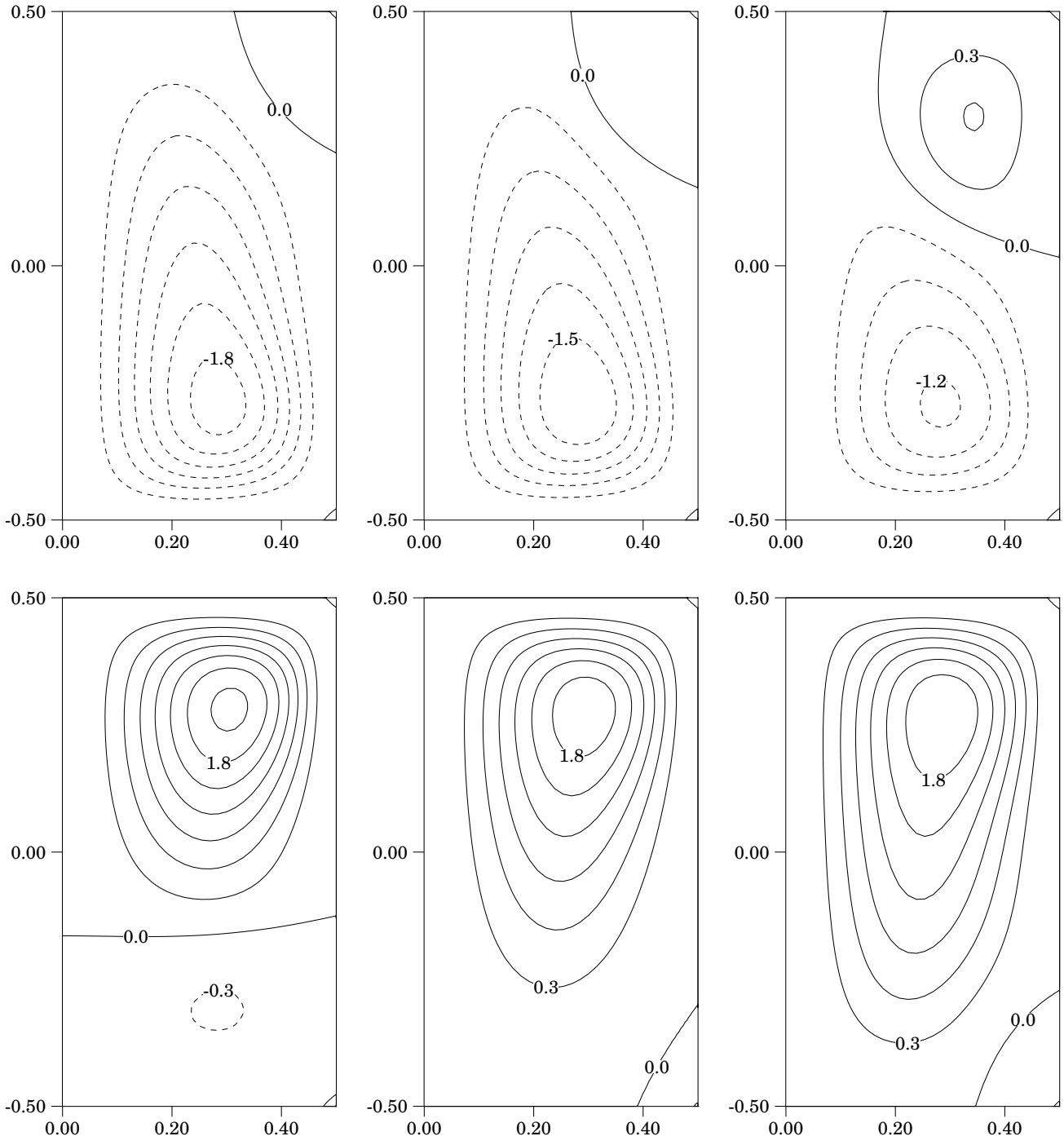

Figure 8: Stream function contours of the $Ra = 8.491 \times 10^4$ osc_1 pure fluid flow at instants $t = 0,\ 0.75,\ 0.8,\ 0.825,\ 0.85, 1$ of Fig. 7.

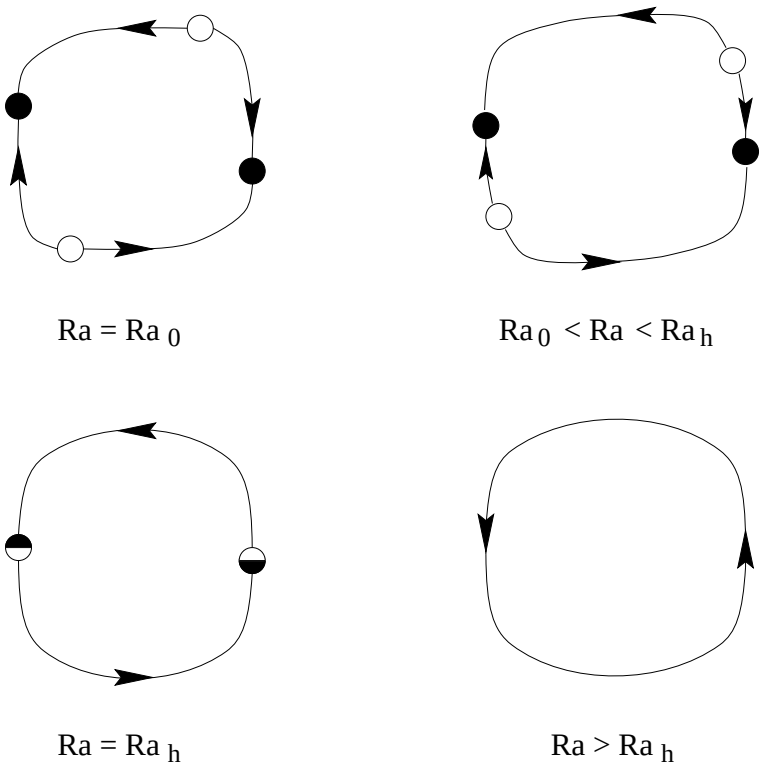

Figure 9: Schematic representation of the global bifurcation involving pairs of stable (solid dots) and unstable (hollow dots) steady states and leading to the generation of a limit cycle: For a given value of the control parameter (Ra_0) two pairs of stable and unstable nodes coexist in phase space, their in-sets and out-sets connected in a heteroclinic orbit. As Ra is increased towards Ra_h, stable and unstable nodes approach one another (pairwise). At Ra_h, they merge (and vanish) in saddle-node bifurcations and the heteroclinic orbit becomes a limit cycle for $Ra > Ra_h$.

binary liquid sta_1 flows do not likewise bifurcate towards oscillatory osc_1-like states. This is in fact due to the occurrence of bifurcations of different type in each case. For the binary liquid sta_1 flows, when Ra is slightly below the threshold $Ra_c = 1.0803 \times 10^4$, the relaxation to steadiness consists of exponentially decaying oscillations that can be fitted by $e^{\lambda t} \cos \omega t$. This implies that these sta_1 fixed points are spiral nodes. The decay rates λ and frequencies ω are moreover found to follow the $(\lambda(Ra), \omega(Ra)) \propto (Ra_c - Ra)$ scaling expected in the vicinity of a Hopf bifurcation which turns out to be subcritical (see Fig. 2). In particular, $\omega(Ra_c) = 24.3$, a value rather close to that at the Hopf bifurcation of the quiescent state $\omega = 28.84$ ([11]). Why should the quiescent state stability be related to the presently discussed transition? Although we are unable to even begin answering that, let us mention the observation by [1], in 2D extended rectangular cells, of switching travelling-waves, where transient regions of convection (of frequency also very close to that observed at the Hopf bifurcation of the quiescent layer) appear in corners and spread over the cell.

3.2.5 Physical analysis of the sta_1 flows' destabilization

Going from a detailed description of the differences between the pure and binary sta_1 states bifurcations to a physical insight on the underlying mechanisms is by no way easy. Only some clues can be proposed, which is the topic of this section.

As previously pointed out, even though the sta_1 flows are similar, the corresponding

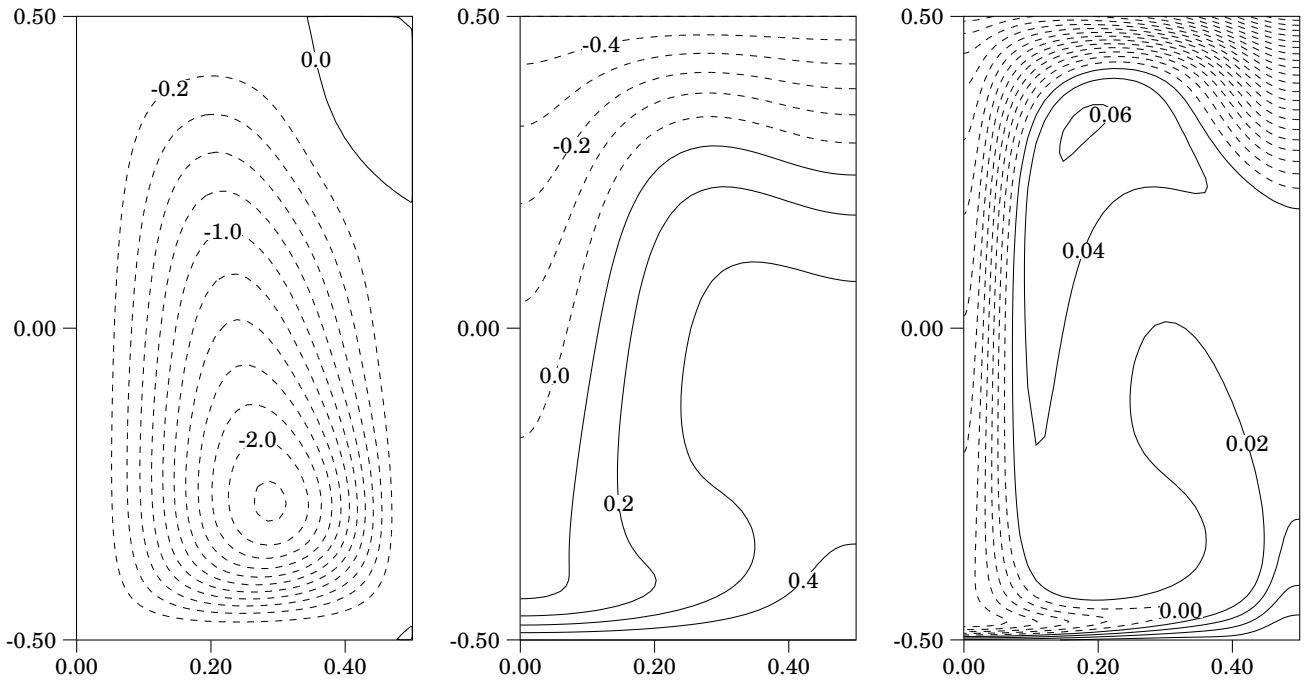

Figure 10: Stream function, temperature $T = \Theta_S(z) + \theta(r, z)$ and mass fraction $C = \Gamma_S(z) + \gamma(r, z)$ contours of the $Ra = 1.075 \times 10^5$ binary liquid sta_1 steady state (NS configuration).

fixed points are of different types and undergo different bifurcations. In other words, merely observing similar flows cannot lead to any conclusion as to their upcoming transitions.

Nevertheless, going back to the analysis of their similarities, we find that in the top corner region (see Figs. 6 and 10) both temperature and mass fraction fields are almost vertically stratified. The temperature distributions along the sidewall of the enclosure of pure fluid sta_1 states are shown in the upper graph of Fig. 11, for various Ra values below Ra_c. Surprisingly, these do not evolve much in the range in Ra over which a significant growth of the corner roll is observed. The same behavior occurs in the binary liquid sta_1 states, for the temperature and mass fraction, as shown in the lower graph of Fig. 11. The corresponding 'buoyancy' profile $T + \Psi C$ is therefore also stratified. These results imply that in both cases local 'buoyancy' gradients are approximately constant for $z \in [0.2, 0.5]$.

The next step of the analysis comes from the following observations:

- Velocities in the corner roll are small compared to those of the main roll (typically by a factor of twenty or more), which leads to admit that the fluid layer is locally quasi-quiescent.

- The evolution of the corner roll height h with Ra is displayed in Fig. 12. To be specific, h was computed as being the distance between the upper corner of the enclosure ($r = 0.5$, $z = 0.5$) and the altitude at which the null stream function contour (that marks the separation between main and corner rolls) reaches the sidewall. The $h(Ra)$ graph of Fig. 12 shows that for both pure and binary liquid systems, h is less than 0.3, which implies that the corner rolls dwell in regions where 'buoyancy' gradients are essentially constant. Due to the seemingly diverging trend of the $h(Ra)$ curve in Fig. 12, the pure liquid case deserves further comments on that aspect. Indeed, going back to the description of the oscillatory osc_1 flows (Section 3.2.2), the two states the system is cast to, between the rapid switches, have a slow temporal evolution and possess the

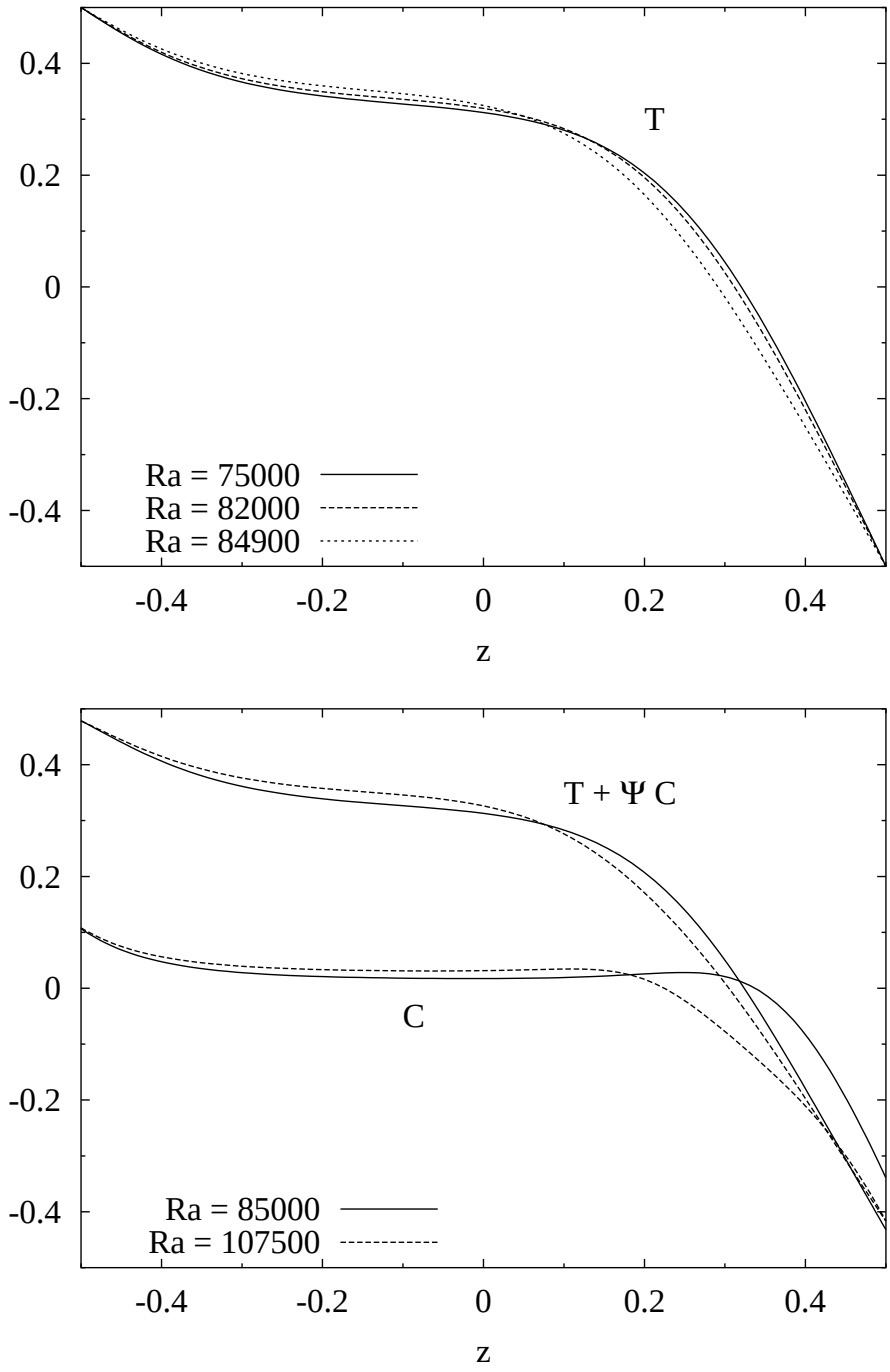

Figure 11: Profiles, taken along the cylinder's circumference, of sta_1 flows (in the NS configuration), at Ra values in the vicinity of the termination de the sta_1 branches of solutions. Upper graph: Temperature $T = \Theta_S(z) + \theta(r, z)$ profile for the pure fluid. Lower graph: Mass fraction $C = \Gamma_S(z) + \gamma(r, z)$ and 'buoyancy' $T + \Psi C$ profiles for the binary liquid.

corner roll and underlying stratification. This supplies an upper bound to the corner roll size just before the bifurcation, evaluated to be 0.28 (see Fig. 8).

These observations imply that a local Rayleigh number $Ra^\star$, based on both h and the local buoyancy gradient, could be assigned to the quasi-quiescent region. As Ra increases, so does h and consequently $Ra^\star \propto h^4$, which implies that the greater the extension of the

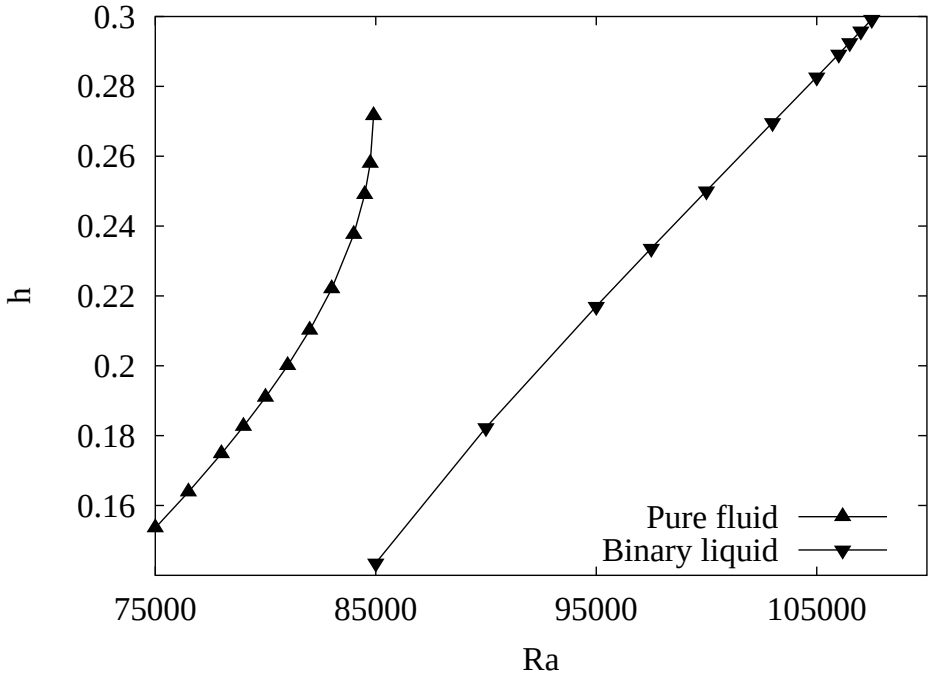

Figure 12: Height h of the corner roll in pure fluid and binary liquid sta_1 flows (NS configuration).

quasi-quiescent region is, the less stable it will be. Eventually h becomes such that the quasi-quiescent region turns unstable (in other words, $Ra^\star$ reaches a critical value), leading to the growth of the corner cell that destabilizes the sta_1 state.

The quiescent region's stability is therefore expected to play some role in the destabilization of these flows. In that respect, it is understandable, and observed, that it occurs for a larger corner roll height (0.3) in a negative separation ratio binary liquid than in a pure fluid. It may furthermore be inferred that such Soret induced behavior will hold for negative and positive Ψ, as well as in 3D configurations.

It might be worth mentioning that the steady convective states shown in [14] also display the presence of a corner roll and its growth with increasing Ra as the transition to oscillatory convection is reached.

4 Conclusions

The axisymmetric convective states of $Pr = 1$ pure and binary liquids (with $\psi = -0.2$ and $Le = 0.1$ for the mixture) enclosed in a small aspect ratio cylinder have been computed for two types of kinematic boundary conditions on the cylinder's circumference, free-slip or no-slip.

When the lateral boundary condition is set to free-slip, high Ra pure fluid and binary liquid steady flows are found to be identical, as pointed out in many other studies (such as [8, 5]).

When the lateral boundary condition is set to no-slip, multiple branches of solutions arise, in both kinds of fluid systems. All the convective solutions, which include steady

and periodic motion, of the binary liquid have analogues in the pure fluid system. There is however a branch of osc_1 periodic oscillations that arises only in the pure fluid system, emerging from an sta_1 steady states branch via a global bifurcation. In the binary liquid system, such a bifurcation does not occur (a subcritical Hopf bifurcation arises instead), and consequently neither does any osc_1-like solution.

The different evolution of the nevertheless similar sta_1 states is related to the presence of a destabilizing buoyancy gradient quasi-quiescent region, and therefore sensitive to the Soret effect in the binary case.

From these results, we conjecture that the steady convective states of pure and binary liquids will indeed become identical at high Ra values if the kinematic and dynamic configurations forbid the formation of locally quasi-quiescent regions of vertically stratified density.

Acknowledgments

We gratefully acknowledge the Centre de Ressources Informatiques de l'Université Paris-Sud for granting us unbounded use of their computer facilities.

References

[1] C.M. Aegerter and C.M. Surko, "Effects of lateral boundaries on travelling-waves dynamics in binary fluid convection" Phys. Rev. E **63**, 046301 (2001).

[2] E. Bodenschatz , W. Pesch and G. Ahlers, "Recent developments in Rayleigh-Bénard convection," Annu. Rev. Fluid Mech. **32**, 709 (2000).

[3] J.K. Platten and J.C. Legros, *Convection in Liquids* (Springer Verlag, Berlin, 1984).

[4] M.C. Cross and P.C. Hohenberg, "Pattern formation outside of equilibrium," Rev. Mod. Phys. **65**, 851 (1993).

[5] M. Lücke, W. Barten, P. Büchel, C. Fütterer, C. Hollinger, and CH. Jung, "Pattern formation in binary fluid convection and in systems with throughflow," in *Evolution of structures in dissipative continuous systems*, edited by F. H. Busse and S. C. Müller (Springer, 1998).

[6] P. Kolodner, S. Slimani, N. Aubry, and R. Lima, "Characterization of dispersive chaos and related states of binary-fluid convection," PHYSICA D **85**, 165 (1995).

[7] W. Barten, M. Lücke, W. Hort and M. Kamps, "Convection in binary fluid mixture. I. Extended traveling-wave and stationary states," Phys. Rev. E **51**, 5636 (1995).

[8] D. Bensimon, A. Pumir and B.I. Shraiman, "Nonlinear Theory of Traveling Wave Convection in Binary Mixtures," J. Phys. France **50**, 3089 (1989).

[9] H. Touiri, J.K. Platten and G. Chavepeyer, "Effect of the seperation ratio on the transition between travelling waves and steady convection in the two-component Rayleigh-Bénard problem," Eur. J. Mech./B Fluids **11**, 2078 (1996).

[10] A. La Porta, K.D. Eaton and C.M. Surko, "Transition between curved and angular textures in binary fluid convection," Phys. Rev. E **53**, 570 (1996).

[11] E. Millour and G. Labrosse, E. Tric, "Sensitivity of binary liquid thermal convection to confinement," Phys. Fluids **15**, 2791 (2003).

[12] M. Wanschura, H. C. Kuhlmann, and H. J. Rath, "Three-dimensional instability of axisymmetric buoyant convection in cylinders heated from below," J. Fluid Mech. **326**, 399 (1996).

[13] G.S. Charlson and R.L. Sani, "On thermoconvective instability in a bounded cylindrical fluid layer," Int. J. Heat Mass Transfer **14**, 2157 (1970).

[14] L.S. Tuckerman and D. Barkley, "Global bifurcation to traveling waves in axisymmetric convection," Phys. Rev. Lett. **61**, 408 (1988).

[15] D. Barkley and L. Tuckerman, "Traveling waves in axisymmetric convection: the role of sidewall conductivity," Physica D **37**, 288 (1989).